# Anisotropic Surface Broadening and Core Depletion during the Evolution of a Strong-Field Induced Nanoplasma

Camila Bacellar,[1,2,*] Adam S. Chatterley,[1,2,†] Florian Lackner,[1,2,‡] C. D. Pemmaraju,[1,§] Rico Mayro P. Tanyag,[3,†] Deepak Verma,[3] Charles Bernando,[4] Sean M. O. O'Connell,[3,‖] Maximilian Bucher,[5] Ken R. Ferguson,[6] Tais Gorkhover,[6,7,8,¶] Ryan N. Coffee,[6] Giacomo Coslovich,[6] Dipanwita Ray,[6] Timur Osipov,[6] Daniel M. Neumark,[1,2] Christoph Bostedt,[5,6,9,*,**] Andrey F. Vilesov,[3,4,††] and Oliver Gessner[1,‡‡]

[1]*Chemical Sciences Division, Lawrence Berkeley National Laboratory, Berkeley, California 94720, USA*
[2]*Department of Chemistry, University of California Berkeley, Berkeley, California 94720, USA*
[3]*Department of Chemistry, University of Southern California, Los Angeles, California 90089, USA*
[4]*Department of Physics and Astronomy, University of Southern California, Los Angeles, California 90089, USA*
[5]*Argonne National Laboratory, 9700 South Cass Avenue B109, Lemont, Illinois 60439, USA*
[6]*Linac Coherent Light Source, LCLS, SLAC National Accelerator Laboratory, 2575 Sand Hill Road, Menlo Park, California 94025, USA*
[7]*Institute of Optics and Atomic Physics, Technical University of Berlin, Hardenbergstraße 36, 10623 Berlin, Germany*
[8]*Stanford PULSE Institute, SLAC National Accelerator Laboratory, 2575 Sand Hill Road, Menlo Park, California 94025, USA*
[9]*Department of Physics and Astronomy, Northwestern University, 2145 Sheridan Road, Evanston, Illinois 60208, USA*

(Received 15 September 2021; revised 30 April 2022; accepted 29 June 2022; published 12 August 2022)

Strong-field ionization of nanoscale clusters provides excellent opportunities to study the complex correlated electronic and nuclear dynamics of near-solid density plasmas. Yet, monitoring ultrafast, nanoscopic dynamics in real-time is challenging, which often complicates a direct comparison between theory and experiment. Here, near-infrared laser-induced plasma dynamics in ~600 nm diameter helium droplets are studied by femtosecond time-resolved x-ray coherent diffractive imaging. An anisotropic, ~20 nm wide surface region, defined as the range where the density lies between 10% and 90% of the core value, is established within ~100 fs, in qualitative agreement with theoretical predictions. At longer timescales, however, the width of this region remains largely constant while the radius of the dense plasma core shrinks at average rates of ≈71 nm/ps along and ≈33 nm/ps perpendicular to the laser polarization. These dynamics are not captured by previous plasma expansion models. The observations are phenomenologically described within a numerical simulation; details of the underlying physics, however, remain to be explored.

DOI: 10.1103/PhysRevLett.129.073201

Studying strong-field ionization (SFI) of nanoclusters yields a better understanding of the coupled electronic-nuclear dynamics underlying nanoplasma formation and evolution. Until recently, real-time access to these dynamics, which typically proceed on femtosecond to picosecond temporal and nanometer spatial scales, was challenging. Most experiments focused on electron and ion kinetic energy and momentum distributions, which superimpose signals from all stages of the nanoplasma evolution [1–12]. X-ray free electron lasers (XFELs) and intense high-order harmonic generation (HHG) light sources have enabled a new class of single-shot coherent diffractive imaging (CDI) experiments that probe transient plasma shapes and electron density distributions in real time and with $< 100$ fs temporal resolution [13–22]. CDI experiments by Gorkhover *et al.* demonstrated that SFI of $Xe_N$ clusters, $\sim 30 - 60$ nm in diameter, with near-infrared (NIR) laser pulses at $\approx 2 \times 10^{15}$ W/cm$^2$ induces an increased surface width [15], instead of a previously suggested uniform cluster expansion [1,2]. A time-resolved wide-angle x-ray scattering (WAXS) study by Ueda and co-workers supports this picture and provides additional insight into the loss of crystalline order [21]. Microscopic particle-in-cell (MicPIC) calculations predict a similar surface broadening process in a nanoplasma generated by SFI of ~50 nm diameter hydrogen clusters [23]. Additionally, the calculations yield an enhanced surface width along the laser polarization compared to perpendicular directions, and a few percent surface anisotropy that persists for at least ~100 fs during the hydrodynamic expansion [23]. Electron and ion energy and momentum distributions resulting from SFI of nanoclusters provided evidence for anisotropic nanoplasma processes [24–32]. However, monitoring the emergence and evolution of anisotropies in real time has not yet been achieved. We use ultrafast CDI to reveal pronounced anisotropic nanoplasma dynamics that emerge within the ≈40 fs laser pulse duration and continue to evolve on picosecond timescales. The results reproduce a

 

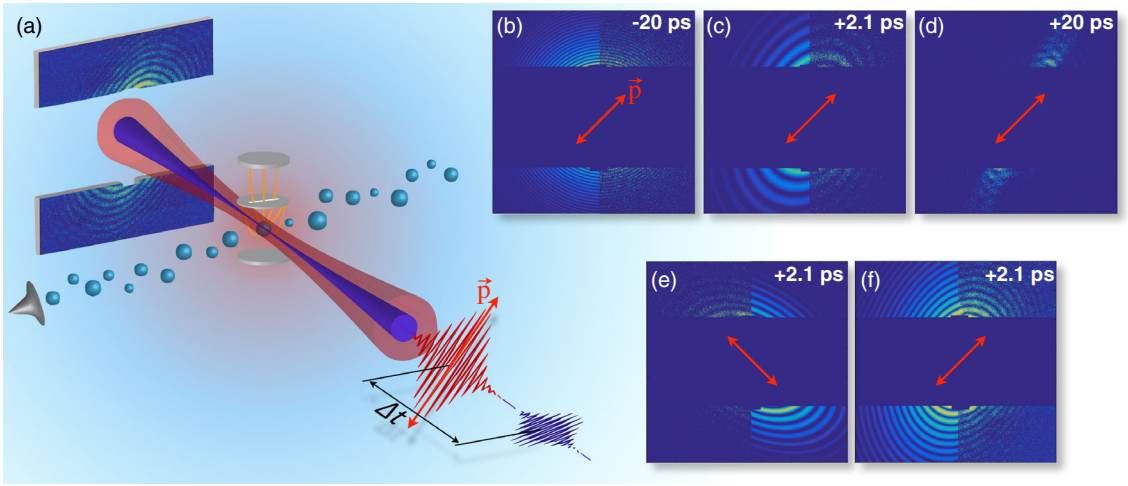


FIG. 1. (a) Nanoplasmas are generated by exposing helium nanodroplets to an intense, linearly polarized NIR pulse (red). The temporal evolution of the plasmas is probed via coherent x-ray scattering using a delayed x-ray pulse (blue). (b)–(d) Representative scattering patterns for three pump-probe delays of −20 (b), 2.1 (c), and 20 ps (d) at a constant NIR polarization (red arrows). (e), (f) Patterns recorded with two different NIR polarizations at $\Delta t = 2.1$ ps. In each panel, the scattered points in two of the four quadrants are experimental data, whereas the smooth lines in the other two quadrants are fits as described in the text.

predicted anisotropic surface broadening during the laser-plasma interaction [23] and reveal saturation of the surface width after ∼100–200 fs as well as a pronounced anisotropic shrinking of the plasma core on timescales of up to tens of picoseconds.

A schematic of the experimental setup at the Linac Coherent Light Source (LCLS) AMO instrument is shown in Fig. 1(a) [33]. Helium droplets with an average radius $R \approx 300$ nm are generated by continuous expansion of He fluid at 20 bar through a cold (4.7 K) 5 $\mu$m wide nozzle [34]. The droplet beam is intercepted by NIR laser pulses ($\lambda = 800$ nm, duration $\tau \approx 40$ fs, focal size $2w \approx 75$ $\mu$m) at intensities of $\approx 3$–$4 \times 10^{15}$ W/cm$^2$, leading to the formation of nanoplasmas by SFI [35]. The plasma temporal evolution is monitored by recording x-ray diffraction patterns, each generated by the interaction of a single x-ray pulse ($\lambda = 2.07$ nm, $\tau \approx 100$ fs, $2w \approx 3$–$5$ $\mu$m) [36] with a single droplet. For each diffraction pattern, an ion time-of-flight (TOF) spectrum is recorded in coincidence, from which the degree of ionization and the ion kinetic energy distribution are obtained. This procedure, as well as more experimental details are outlined in the Supplemental Material [37], which includes Refs. [38–49].

Representative diffraction patterns from three different time delays are shown in Figs. 1(b)–1(d). At negative and small positive delays (≲300 fs), the vast majority of images consist of a series of concentric rings, indicating predominantly spherical droplet shapes [13] [Fig. 1(b)]. At 2.1 ps delay, however, strongly elliptical patterns are observed with their long axes aligned along the NIR polarization [Fig. 1(c)]. After 20 ps, only streaked images are observed with intensities strongly concentrated along the NIR polarization [Fig. 1(d)]. Note that for a nominal NIR polarization angle of +45° (clockwise), an additional offset angle of ∼23° is observed between the patterns and the nominal polarization axis. The offset is ascribed to accidental polarization control in the optical beam path, as discussed in Sec. II.C of the Supplemental Material [37]. Rotation of the NIR polarization by 90° leads to a corresponding rotation of the elliptical patterns as demonstrated in Figs. 1(e) and 1(f). A more detailed discussion of the relative abundances of various patterns is provided in the Supplemental Material [37].

X-ray diffraction patterns are sensitive to electron density distributions. Based on calculations for hydrogen clusters [23], we assume that electron and ion density distributions become very similar within less than ∼100 fs and, therefore, that the diffraction images largely reflect the distributions of both electrons and ions of quasineutral plasmas. The observed elliptical patterns [Figs. 1(c), 1(e), and 1(f)] are modeled by diffraction from spheroids (smoothed lines) in very good agreement with the experiment [13,37]. For spheroidal shapes with a sharp surface, the scattering intensity scales as $I(q,\Phi) \sim q^{-4} cos^2(qR_{\mathrm{eff}})$, where $q = |\vec{q}|$ is the modulus of the scattering vector, $\Phi$ is the azimuthal angle in the detector plane, and $R_{\mathrm{eff}}$ is the $\Phi$ dependent radius of the spheroid's projection onto the detector (see Supplemental Material [37] for an in-depth discussion, which includes Refs. [13,50–53]). This $q$ dependence is readily apparent in Fig. 2(a), which shows the azimuthally integrated quantity $Iq^4$ for a diffraction image at negative pump-probe delay, i.e., for an unperturbed spherical droplet with a sharp surface [54,55]. In contrast, Fig. 2(b) shows the same quantity for a droplet 74 fs after interaction with the NIR pulse. In this case, the intensity drops faster than $q^{-4}$, and is well captured by a modified description $I(q,\Phi) \sim q^{-\alpha} cos^2(qR_{\mathrm{eff}})$ with $\alpha \approx 5.5$. Values of $\alpha > 4$

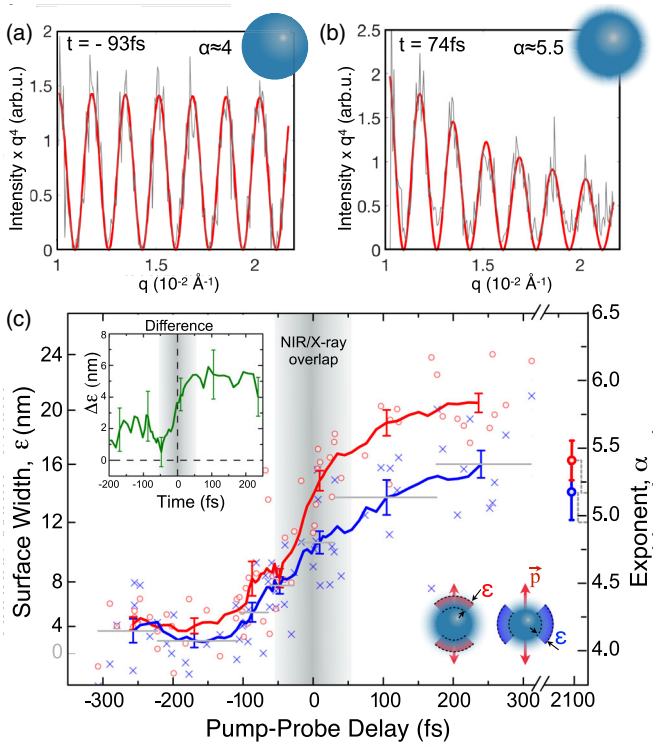


FIG. 2. (a), (b) Power-law fits (red) of azimuthally integrated scattering patterns (gray), indicating exponents of (a) $\alpha \approx 4$ before and (b) $\alpha \approx 5.5$ after the laser-droplet interaction. Intensities are scaled by $q^4$ for improved clarity. (c) Temporal evolution of the exponents $\alpha$ (right) and corresponding surface widths $\varepsilon$ (left) for 90° wide angular ranges parallel (red) and perpendicular (blue) to the NIR polarization axis. Circles and crosses mark individual data points, lines represent 10-point moving averages. Note that the exponent values on the right ordinate apply to all data points except those at 2.1 ps delay, whose values are indicated by the dotted gray lines. The left ordinate applies to all data. Exemplary vertical error bars indicate uncertainties of the mean values, horizontal gray lines indicate corresponding 10-point averaging ranges. The inset shows the average difference between parallel and perpendicular surface widths (green). Gray-shaded areas indicate the nominal NIR–x-ray pulse overlap.

indicate that the plasma surface is not sharp but has a finite width $\varepsilon$, defined as the range over which the density drops from 90% to 10% of the interior value. For each droplet or nanoplasma, the width $\varepsilon$ is obtained from the measured decay exponent $\alpha$. The required $\varepsilon - \alpha$ relationship is derived in two steps. First, the radial droplet density distribution is modeled by a modified Fermi function [16,23], and simulated diffraction patterns are calculated for a variety of droplet sizes, shapes, and surface widths. Next, the radial intensity distributions of the simulated patterns are fit to the description given above, providing a unique value $\alpha$ for each $\varepsilon$, and vice versa. Corresponding calibration curves are shown in Fig. S7 of the Supplemental Material [37], including a discussion of the fitting procedure and uncertainty estimates [56].

Figure 2(c) shows the decay exponents $\alpha$ (right) and surface widths $\varepsilon$ (left) for scattering intensities averaged over $\Delta\Phi = 90°$ wide slices parallel (red) and perpendicular (blue) to the NIR polarization. Figure 2(c) reveals that, for delays $\Delta t < 300$ fs, $\varepsilon$ increases monotonically in both parallel and perpendicular directions. Additionally, at the peak of the NIR pulse around time zero, a difference in surface widths, $\Delta\varepsilon$, of approximately 4–5 nm is established within less than 100 fs and remains constant throughout the continued surface broadening [Fig 2(c) inset]. After ~100–200 fs, the surface widths saturate at values of ≈21 nm at the poles (along the NIR polarization) and ≈16 nm at the equator. Similar, albeit slightly smaller surface widths are observed at 2.1 ps delay. The saturation of the surface width after a few hundred femtoseconds is contrasted by a very pronounced, continuous shape change of the droplet core as evidenced by the strongly elliptical patterns at 2.1 ps [Figs. 1(c), 1(e), and1(f)] and streaks at 20 ps [Fig. 1(d)]. The increase of the average diffraction ring spacing shows that the droplet core does not expand, as expected from previous models [1,2], but instead shrinks with increasing time delay, as recently reported elsewhere [15,16,23].

Interestingly, up to ~100 fs, the average surface broadening rates of $\sim 70 - 95$ nm/ps observed here are remarkably close to the ~70 nm/ps predicted by Fennel and co-workers for smaller hydrogen clusters [23] ($H_N$,$N \approx 3 \times 10^6$). Additionally, the difference $\Delta\varepsilon$ between the polar and equatorial surface widths is essentially established within the NIR pulse duration and remains constant thereafter in both theory and experiment [Fig. 3b in Ref. [23] and Fig. 2(c)]. The asymptotic difference is ~5 nm for the He droplets compared to ~1.4 nm in the $H_N$ clusters. The surface anisotropy is predominantly ascribed to enhanced Coulomb explosion at the poles due to reduced ion screening during the oscillatory plasma electron motion in the laser field [23,27]. The laser intensity in the He droplet experiment is approximately four times higher than in the $H_N$ cluster calculation, which may lead to larger oscillation amplitudes and stronger Coulomb repulsion effects [57]. Thus, the observed anisotropic plasma surface dynamics up to ~100 fs qualitatively reproduce theoretical predictions. The saturation of the surface width and the pronounced core anisotropies emerging on picosecond timescales, however, are unexpected and represent key new insights revealed by this study. Calculations [23] do not indicate a saturation of the surface width. However, they are restricted to delays ≤100 fs, where saturation effects in the experimental data presented here are also very limited [Fig. 2(c)]. Gorkhover *et al.* did not detect any saturation (or anisotropies) up to 500 fs after SFI of small Xe clusters [15]. However, the Xe cluster surface broadens more slowly than the He droplet surface and the relatively small Xe aggregates essentially disintegrate before their surface widths become comparable to the saturation values observed here. The observations described herein, therefore, do not disagree

with previous results but rather extend the range of CDI studies on SFI induced nanoplasmas to previously unexplored timescales and length scales.

A particularly surprising finding is that the core size and shape evolution does not mirror the surface broadening dynamics. During the first 2.1 ps, the core radii drop at average rates of $dR_{\mathrm{para}}/dt \approx -71$ nm/ps and $dR_{\mathrm{perp}}/dt \approx -33$ nm/ps, reducing the droplet diameter from pole to pole to about 2/3 of the equatorial diameter (aspect ratio AR ≈ 1.5). The average droplet radius is reduced by ∼100 nm during this time while the surface width remains nearly constant at ∼15–20 nm [58]. We note that at 2.1 ps, ∼50% of the images exhibit speckled patterns, indicating that there may be alternative plasma evolution mechanisms. Generally, such speckles are associated with highly inhomogeneous objects, such as droplets undergoing disintegration into multiple fragments. Unfortunately, the large gap between the detector panels required in this work renders a reconstruction of the density distributions via a phase retrieval algorithm, as shown in our previous works, unfeasible [19,59,60]. The streaked images recorded at a pump-probe delay of 20 ps are consistent with a continued flattening of the droplet shapes along the NIR polarization on tens of picosecond timescales. Ion TOF spectra show that approximately twice as many ions are ejected parallel to the laser polarization (per unit solid angle) as compared to the perpendicular direction, while the total number of ejected $He^+$ ions is comparable to that of the number of atoms in the droplets. These measurements suggest a continued anisotropic ion ejection well beyond the duration of the laser-droplet interaction. The characteristic ion kinetic energies are also higher along the laser polarization [37]. At 100 ps, no diffraction patterns are detected, indicating that all droplets have disintegrated by then. These findings for large He nanodroplets differ from the suspended expansion observed in comparably sized Xe clusters, for which initial surface peeling is followed by very slow (∼ns) dynamics within a residual, neutral plasma core [16,61,62]. We note that neither nanometer-scale changes in the droplet core sizes nor changes in aspect ratios during the first 300 fs can be directly observed. This is due to the inherent droplet size distribution and the fact that, based on the average anisotropic core shrinking rates, a spherical droplet would acquire an AR of ∼1.04 during this time, which is smaller than the average droplet aspect ratio in the beam. However, the key finding of a continued anisotropic core depletion is supported by the data recorded at 2.1 and 20 ps pump-probe delays and by a statistical analysis of the size distributions for various pump-probe delays as described in Sec. II.B of the Supplemental Material [37].

Detailed theoretical modeling of nanoplasma dynamics comparable to those for smaller hydrogen [23] and xenon [62] clusters is not available for large He nanodroplets. Liseykina and Bauer [63] predicted strongly inhomogeneous, anisotropic ionization dynamics in micrometer sized He droplets exposed to NIR intensities of $5.2 \times 10^{17}$ W/cm$^2$. Anisotropic ionization may also contribute to the dynamics observed here. However, the starkly different excitation regimes make a direct comparison challenging [37]. In the absence of a bottom-up description, we resort to a numerical mass-flow simulation to provide a self-consistent interpretation of the observed scattering patterns and TOF spectra that obeys basic laws of mass and energy conservation. A detailed description of the simulation is given in the Supplemental Material Sec. IV.A [37], which includes Refs. [1,2,5,23–25,27–32,64–68]. Briefly, the simulation is based on the assumption that the shape evolution is predominantly driven by ion ejection from the plasma surface, in agreement with other theoretical [23,62] and experimental [15,21,62] works. The average velocity by which ions move away from the plasma center is assumed to be related to the local density and its gradient, approaching zero effective radial velocity inside the droplet bulk and maximum radial velocity in the free atom limit. Within this picture, an instantaneous radial density profile can be translated into an effective radial velocity profile, which in turn affects the further evolution of the density profile. Numerical propagation of the density distribution and the effective mass transport away from the droplet yields the simulation results displayed in Fig. 3. We emphasize that this simulation is mostly phenomenological and based on a set of adjustable parameters. The underlying physics, such as time-dependent charge and energy distributions and the relative contributions of hydrodynamic expansion and Coulomb explosion dynamics, remains to be explored by significantly more sophisticated calculations. The simulation does, however, provide a consistent description of the experimentally observed scattering images and TOF spectra.

Figure 3(a) compares the average measured density profiles along (orange) and perpendicular to (light blue) the NIR polarization with the simulation (red and blue shaded areas). Note that the stretched-out pedestals at large $r$ cannot be detected in the current experiment and may lead to an underestimation of the surface width by up to 30% [37]. The free atom velocities in the simulations correspond to kinetic energies of 500 and 100 eV for parallel and perpendicular directions, respectively. These energies are chosen such that they are consistent with the differences between kinetic energy distributions measured parallel and perpendicular to the NIR polarization [37]. Figure 3(b) shows three-dimensional renderings of the simulated density profiles. The simulation captures the key aspects of the observed plasma shape evolution, i.e., the saturation of surface width within hundreds of femtoseconds and the continued anisotropic shrinking of the high-density core. Anisotropies in ion emission intensities and kinetic energies from SFI induced nanoplasmas have previously been reported by a number of groups [24–31]. However, these anisotropies were recorded by time-integrated techniques

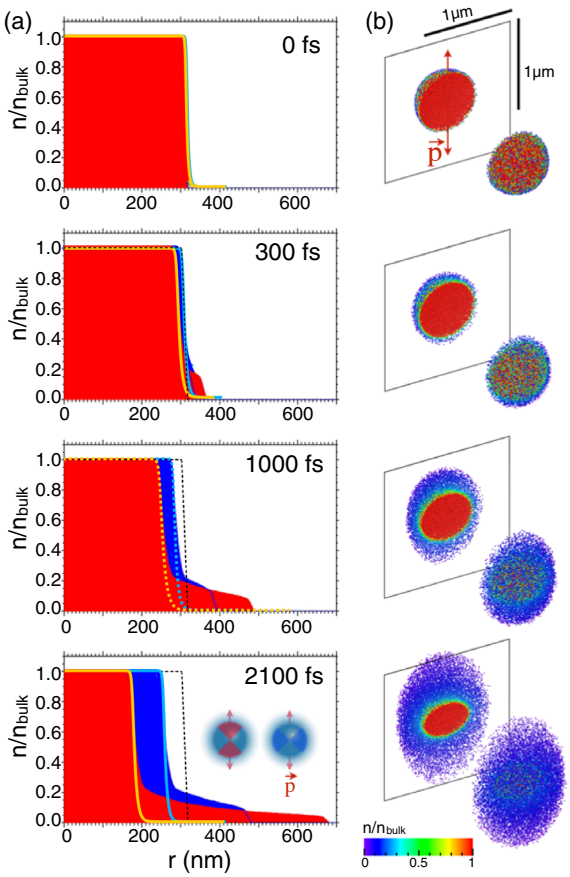


FIG. 3. (a) Plasma electron density profiles parallel (red) and perpendicular (blue) to the NIR polarization as a function of pump-probe delay. Solid orange and light blue lines are determined experimentally, shaded areas by a numerical model. The dashed lines at 1000 fs delay are interpolations of experimental data at 300 fs and 2100 fs. The dotted black lines in the lower three panels indicate the original density profile. The inset in the bottom panel indicates the angular integration ranges for the experimental data. (b) Simulated nanoplasma density evolution. Densities are represented by the density of points as well as their colors according to the color bar. The 3D patterns are cut in half in the indicated plane and the front halves are offset to reveal the radial density profiles.

that do not provide direct access to dynamics during and after the laser-plasma interaction. The study presented here closes this gap, revealing a significantly more detailed picture of the ultrafast, nanoscale dynamics underlying the final product distributions.

In summary, this Letter provides real-time measurements of the evolution of an anisotropic nanoplasma. An anisotropic plasma surface appears within ~100 fs and saturates within ~300 fs after SFI with characteristic widths of ~20 nm parallel and ~15 nm perpendicular to the strong field polarization. The observed dynamics are in qualitative agreement with theoretical predictions for hydrogen clusters. While the surface width remains almost constant for at least 2.1 ps, the shape of the plasma core changes significantly during the same period, shrinking by ~45% and ~19% in parallel and perpendicular directions, respectively. A numerical model reproduces the observed trends, the underlying physics, however, remains to be explored. We hope that the experimental benchmarks and phenomenological framework provided may stimulate renewed efforts to extend the detailed theoretical modeling of strong-field induced nanoplasma dynamics toward larger systems and longer timescales, ultimately bridging the gap between the few-atom limit and macroscopic plasma phenomena.

Raw data were generated at the Linac Coherent Light Source (LCLS) large-scale facility. Derived data supporting the findings of this study are available from the corresponding author upon request.

This research was supported by the U.S. Department of Energy (DOE), Office of Science, Office of Basic Energy Sciences (BES), Chemical Sciences, Geosciences and Biosciences Division, through Contract No. DE-AC02-05CH11231 (C. Ba., A. S. C., C. D. P., D. M. N., O. G.), and Contract No. DE-AC02-06CH11357 (M. B., C. Bo.). A. F. V. was supported by NSF Grants No. DMR-1701077 and No. DMR-1501276. F. L. acknowledges support by the Austrian Science Fund (FWF, Erwin Schrödinger Fellowship Grant No. J 3580-N20). T. G. acknowledges support by the P. Ewald fellowship of the Volkswagen Foundation and the Panofsky fellowship of SLAC National Accelerator Laboratory. Portions of this research were carried out at the LCLS, a national user facility operated by Stanford University on behalf of the U.S. DOE, Office of Science, Office of BES under beam-time Grant No. LJ54. Use of the Linac Coherent Light Source (LCLS), SLAC National Accelerator Laboratory, is supported by the U.S. DOE, Office of Science, Office of BES under Contract No. DE-AC02-76SF00515. The authors would like to thank Thomas Fennel and Christian Peltz for helpful advice during the early stages of the image analysis. O. G., A. F. V., and C. Bo. conceived the experiment, C. Ba., A. S. C, F. L., C. D. P., R. M. P. T., C. Be., D. V., S. O'C., M. B., K. R. F., T. G., R. N. C., G. C., D. R., T. O., C. Bo., A. F. V., and O. G. carried out the experiment. C. Ba., A. S. C, C. Be., A. F. V., and O. G. performed the data analysis and theoretical modeling. C. Ba., A. S. C, F. L., R. M. P. T., T. G., G. C., D. M. N., C. Bo., A. F. V., and O. G wrote the manuscript. The authors declare no competing financial interests.

*Present address: Paul Scherrer Institut, Forschungsstrasse 111, 5232 Villigen-PSI, Switzerland.
†Present address: Department of Chemistry, Aarhus University, Langelandsgade 140, 8000 Aarhus C, Denmark.
‡Present address: Institute of Experimental Physics, Graz University of Technology, Petersgasse 16, A-8010 Graz, Austria.
§Present address: IBM, San Jose, California 95141, USA.

[‖]Present address: University of Miami Rosenstiel School of Marine and Atmospheric Science, Miami, Florida 33149, USA.
[¶]Present address: University of Hamburg, Center for Free-Electron Laser Science, Luruper Chaussee 149, 22761 Hamburg, Germany.
[**]Corresponding author.
christoph.bostedt@psi.ch
[††]Corresponding author.
vilesov@usc.edu
[‡‡]Corresponding author.
ogessner@lbl.gov

[1] T. Ditmire, T. Donnelly, A. M. Rubenchik, R. W. Falcone, and M. D. Perry, Interaction of intense laser pulses with atomic clusters, Phys. Rev. A **53**, 3379 (1996).
[2] T. Ditmire, J. W. G. Tisch, E. Springate, M. B. Mason, N. Hay, J. P. Marangos, and M. H. R. Hutchinson, High Energy Ion Explosion of Atomic Clusters: Transition from Molecular to Plasma Behavior, Phys. Rev. Lett. **78**, 2732 (1997).
[3] M. Lezius, S. Dobosz, D. Normand, and M. Schmidt, Explosion Dynamics of Rare Gas Clusters in Strong Laser Fields, Phys. Rev. Lett. **80**, 261 (1998).
[4] U. Saalmann, C. Siedschlag, and J. M. Rost, Mechanisms of cluster ionization in strong laser pulses, J. Phys. B **39**, R39 (2006).
[5] T. Fennel, K. H. Meiwes-Broer, J. Tiggesbäumker, P. G. Reinhard, P. M. Dinh, and E. Suraud, Laser-driven nonlinear cluster dynamics, Rev. Mod. Phys. **82**, 1793 (2010).
[6] K. Ostrikov, F. Beg, and A. Ng, Colloquium: Nanoplasmas generated by intense radiation, Rev. Mod. Phys. **88**, 011001 (2016).
[7] B. Schütte, M. Arbeiter, A. Mermillod-Blondin, M. J. J. Vrakking, A. Rouzée, and T. Fennel, Ionization Avalanching in Clusters Ignited by Extreme-Ultraviolet Driven Seed Electrons, Phys. Rev. Lett. **116**, 033001 (2016).
[8] M. Kelbg, M. Zabel, B. Krebs, L. Kazak, K. H. Meiwes-Broer, and J. Tiggesbäumker, Temporal Development of a Laser-Induced Helium Nanoplasma Measured through Auger Emission and Above-Threshold Ionization, Phys. Rev. Lett. **125**, 093202 (2020).
[9] T. Döppner, T. Diederich, A. Przystawik, N. X. Truong, T. Fennel, J. Tiggesbäumker, and K. H. Meiwes-Broer, Charging of metal clusters in helium droplets exposed to intense femtosecond laser pulses, Phys. Chem. Chem. Phys. **9**, 4639 (2007).
[10] C. Bostedt, H. Thomas, M. Hoener, E. Eremina, T. Fennel, K. H. Meiwes-Broer, H. Wabnitz, M. Kuhlmann, E. Plönjes, K. Tiedtke, R. Treusch, J. Feldhaus, A. R. B. deCastro, and T. Moller, Multistep Ionization of Argon Clusters in Intense Femtosecond Extreme Ultraviolet Pulses, Phys. Rev. Lett. **100**, 133401 (2008).
[11] B. F. Murphy, K. Hoffmann, A. Belolipetski, J. Keto, and T. Ditmire, Explosion of Xenon Clusters Driven by Intense Femtosecond Pulses of Extreme Ultraviolet Light, Phys. Rev. Lett. **101**, 203401 (2008).
[12] S. R. Krishnan, C. Peltz, L. Fechner, V. Sharma, M. Kremer, B. Fischer, N. Camus, T. Pfeifer, J. Jha, M. Krishnamurthy *et al.*, Evolution of dopant-induced helium nanoplasmas, New J. Phys. **14**, 075016 (2012).
[13] L. F. Gomez, K. R. Ferguson, J. P. Cryan, C. Bacellar, R. M. P. Tanyag, C. Jones, S. Schorb, D. Anielski, A. Belkacem, C. Bernando *et al.*, Shapes and vorticities of superfluid helium nanodroplets, Science **345**, 906 (2014).
[14] D. Rupp, M. Adolph, L. Flückiger, T. Gorkhover, J. P. Müller, M. Müller, M. Sauppe, D. Wolter, S. Schorb, R. Treusch *et al.*, Generation and structure of extremely large clusters in pulsed jets, J. Chem. Phys. **141**, 044306 (2014).
[15] T. Gorkhover, S. Schorb, R. Coffee, M. Adolph, L. Foucar, D. Rupp, A. Aquila, J. D. Bozek, S. W. Epp, B. Erk *et al.*, Femtosecond and nanometre visualization of structural dynamics in superheated nanoparticles, Nat. Photonics **10**, 93 (2016).
[16] L. Flückiger, D. Rupp, M. Adolph, T. Gorkhover, M. Krikunova, M. Müller, T. Oelze, Y. Ovcharenko, M. Sauppe, S. Schorb *et al.*, Time-resolved x-ray imaging of a laser-induced nanoplasma and its neutral residuals, New J. Phys. **18**, 043017 (2016).
[17] C. Bostedt, E. Eremina, D. Rupp, M. Adolph, H. Thomas, M. Hoener, A. R. B. de Castro, J. Tiggesbäumker, K. H. Meiwes-Broer, T. Laarmann, H. Wabnitz, E. Plonjes, R. Treusch, J. R. Schneider, and T. Moller, Ultrafast X-Ray Scattering of Xenon Nanoparticles: Imaging Transient States of Matter, Phys. Rev. Lett. **108**, 093401 (2012).
[18] B. Langbehn *et al.*, Three-Dimensional Shapes of Spinning Helium Nanodroplets, Phys. Rev. Lett. **121**, 255301 (2018).
[19] S. M. O. O'Connell, R. M. P. Tanyag, D. Verma, C. Bernando, W. Pang, C. Bacellar, C. A. Saladrigas, J. Mahl, B. W. Toulson, Y. Kumagai, P. Walter, F. Ancilotto, M. Barranco, M. Pi, C. Bostedt, O. Gessner, and A. F. Vilesov, Angular Momentum in Rotating Superfluid Droplets, Phys. Rev. Lett. **124**, 215301 (2020).
[20] D. Rupp, L. Flückiger, M. Adolph, A. Colombo, T. Gorkhover, M. Harmand, M. Krikunova, J. P. Müller, T. Oelze, Y. Ovcharenko *et al.*, Imaging plasma formation in isolated nanoparticles with ultrafast resonant scattering, Struct. Dyn. **7**, 034303 (2020).
[21] T. Nishiyama *et al.*, Ultrafast Structural Dynamics of Nanoparticles in Intense Laser Fields, Phys. Rev. Lett. **123**, 123201 (2019).
[22] D. Rupp, N. Monserud, B. Langbehn, M. Sauppe, J. Zimmermann, Y. Ovcharenko, T. Möller, F. Frassetto, L. Poletto, A. Trabattoni *et al.*, Coherent diffractive imaging of single helium nanodroplets with a high harmonic generation source, Nat. Commun. **8**, 493 (2017).
[23] C. Peltz, C. Varin, T. Brabec, and T. Fennel, Time-Resolved X-Ray Imaging of Anisotropic Nanoplasma Expansion, Phys. Rev. Lett. **113**, 133401 (2014).
[24] V. Kumarappan, M. Krishnamurthy, and D. Mathur, Two-dimensional effects in the hydrodynamic expansion of xenon clusters under intense laser irradiation, Phys. Rev. A **66**, 033203 (2002).
[25] D. R. Symes, M. Hohenberger, A. Henig, and T. Ditmire, Anisotropic Explosions of Hydrogen Clusters under Intense Femtosecond Laser Irradiation, Phys. Rev. Lett. **98**, 123401 (2007).
[26] E. Springate, N. Hay, J. W. G. Tisch, M. B. Mason, T. Ditmire, M. H. R. Hutchinson, and J. P. Marangos, Explosion of atomic clusters irradiated by high-intensity laser

pulses: Scaling of ion energies with cluster and laser parameters, Phys. Rev. A **61**, 063201 (2000).
[27] V. Kumarappan, M. Krishnamurthy, and D. Mathur, Asymmetric High-Energy Ion Emission from Argon Clusters in Intense Laser Fields, Phys. Rev. Lett. **87**, 085005 (2001).
[28] M. Krishnamurthy, D. Mathur, and V. Kumarappan, Anisotropic "charge-flipping" acceleration of highly charged ions from clusters in strong optical fields, Phys. Rev. A **69**, 033202 (2004).
[29] M. Hirokane, S. Shimizu, M. Hashida, S. Okada, S. Okihara, F. Sato, T. Iida, and S. Sakabe, Energy distributions of ions emitted from argon clusters Coulomb-exploded by intense femtosecond laser pulses, Phys. Rev. A **69**, 063201 (2004).
[30] E. Skopalovà, Y. C. El-Taha, A. Zaïr, M. Hohenberger, E. Springate, J. W. G. Tisch, R. A. Smith, and J. P. Marangos, Pulse-Length Dependence of the Anisotropy of Laser-Driven Cluster Explosions: Transition to the Impulsive Regime for Pulses Approaching the Few-Cycle Limit, Phys. Rev. Lett. **104**, 203401 (2010).
[31] D. Mathur, F. A. Rajgara, A. R. Holkundkar, and N. K. Gupta, Strong-field ionization and Coulomb explosion of argon clusters by few-cycle laser pulses, Phys. Rev. A **82**, 025201 (2010).
[32] A. Mikaberidze, U. Saalmann, and J. M. Rost, Laser-Driven Nanoplasmas in Doped Helium Droplets: Local Ignition and Anisotropic Growth, Phys. Rev. Lett. **102**, 128102 (2009).
[33] K. R. Ferguson, M. Bucher, J. D. Bozek, S. Carron, J.-C. Castagna, R. Coffee, G. I. Curiel, M. Holmes, J. Krzywinski, M. Messerschmidt *et al.*, The atomic, molecular and optical science instrument at the linac coherent light source, J. Synchrotron Radiat. **22**, 492 (2015).
[34] H. Buchenau, E. L. Knuth, J. Northby, J. P. Toennies, and C. Winkler, Mass spectra and time-of-flight distributions of helium cluster beams, J. Chem. Phys. **92**, 6875 (1990).
[35] B. Walker, B. Sheehy, L. F. DiMauro, P. Agostini, K. J. Schafer, and K. C. Kulander, Precision Measurement of Strong Field Double Ionization of Helium, Phys. Rev. Lett. **73**, 1227 (1994).
[36] C. Bostedt, J. D. Bozek, P. H. Bucksbaum, R. N. Coffee, J. B. Hastings, Z. Huang, R. W. Lee, S. Schorb, J. N. Corlett, P. Denes *et al.*, Ultra-fast and ultra-intense x-ray sciences: First results from the Linac Coherent Light Source free-electron laser, J. Phys. B **46**, 164003 (2013).
[37] See Supplemental Material at http://link.aps.org/supplemental/10.1103/PhysRevLett.129.073201 for a detailed description of the experiment, data analysis, and dynamics modeling.
[38] L. Strüder, S. Epp, D. Rolles, R. Hartmann, P. Holl, G. Lutz, H. Soltau, R. Eckart, C. Reich, K. Heinzinger *et al.*, Large-format, high-speed, X-ray pnCCDs combined with electron and ion imaging spectrometers in a multipurpose chamber for experiments at 4th generation light sources, Nucl. Instrum. Methods Phys. Res., Sect. A **614**, 483 (2010).
[39] T. Gorkhover *et al.*, Nanoplasma Dynamics of Single Large Xenon Clusters Irradiated with Superintense X-Ray Pulses from the Linac Coherent Light Source Free-Electron Laser, Phys. Rev. Lett. **108**, 245005 (2012).
[40] L. F. Gomez, E. Loginov, R. Sliter, and A. F. Vilesov, Sizes of large He droplets, J. Chem. Phys. **135**, 154201 (2011).
[41] M. R. Bionta, N. Hartmann, M. Weaver, D. French, D. J. Nicholson, J. P. Cryan, J. M. Glownia, K. Baker, C. Bostedt, M. Chollet *et al.*, Spectral encoding method for measuring the relative arrival time between x-ray/optical pulses, Rev. Sci. Instrum. **85**, 083116 (2014).
[42] J. M. Glownia, J. Cryan, J. Andreasson, A. Belkacem, N. Berrah, C. I. Blaga, C. Bostedt, J. Bozek, L. F. DiMauro, L. Fang *et al.*, Time-resolved pump-probe experiments at the LCLS, Opt. Express **18**, 17620 (2010).
[43] W. C. Wiley and I. H. McLaren, Time-of-flight mass spectrometer with improved resolution, Rev. Sci. Instrum. **26**, 1150 (1955).
[44] U. Becker, O. Gessner, and A. Rüdel, Photoelectron scattering in molecules and fullerenes, J. Electron Spectrosc. Relat. Phenom. **108**, 189 (2000).
[45] O. Gessner, Y. Hikosaka, B. Zimmermann, A. Hempelmann, R. R. Lucchese, J. H. D. Eland, P. M. Guyon, and U. Becker, 4 sigma -1 Inner Valence Photoionization Dynamics of NO Derived from Photoelectron-Photoion Angular Correlations, Phys. Rev. Lett. **88**, 193002 (2002).
[46] N. Saito and I. H. Suzuki, Yield of kinetic atomic ion from N2 induced by soft X-Ray absorption, Chem. Phys. Lett. **129**, 419 (1986).
[47] G. M. Roberts, J. L. Nixon, J. Lecointre, E. Wrede, and J. R. R. Verlet, Toward real-time charged-particle image reconstruction using polar onion-peeling, Rev. Sci. Instrum. **80**, 053104 (2009).
[48] B. Jochim, R. Erdwien, Y. Malakar, T. Severt, B. Berry, P. Feizollah, J. Rajput, B. Kaderiya, W. L. Pearson, K. Carnes *et al.*, Three-dimensional momentum imaging of dissociation in flight of metastable molecules, New J. Phys. **19**, 103006 (2017).
[49] W. A. Bryan, S. L. Stebbings, J. McKenna, E. M. L. English, M. Suresh, J. Wood, B. Srigengan, I. C. E. Turcu, J. M. Smith, E. J. Divall *et al.*, Atomic excitation during recollision-free ultrafast multi-electron tunnel ionization, Nat. Phys. **2**, 379 (2006).
[50] C. Bernando *et al.*, Shapes of rotating superfluid helium nanodroplets, Phys. Rev. B **95**, 064510 (2017).
[51] M. Kerker, *The Scattering of Light* (Academic Press, New York, 1969).
[52] T. W. Chen and L. M. Yang, Simple formula for small-angle light scattering by a spheroid, Opt. Commun. **123**, 437 (1996).
[53] J. Als-Nielsen and D. McMorrow, *Elements of Modern X-ray Physics*, 2 ed. (John Wiley & Sons, Ltd, Chichester, UK, 2011).
[54] J. Harms, J. P. Toennies, and F. Dalfovo, Density of superfluid helium droplets, Phys. Rev. B **58**, 3341 (1998).
[55] M. Barranco, R. Guardiola, S. Hernández, R. Mayol, J. Navarro, and M. Pi, Helium Nanodroplets: An Overview, J. Low Temp. Phys. **142**, 1 (2006).
[56] P. J. Cumpson and M. P. Seah, Random uncertainties in AES and XPS: I: Uncertainties in peak energies, intensities and areas derived from peak synthesis, Surf. Interface Anal. **18**, 345 (1992).
[57] T. Pfeifer, C. Spielmann, and G. Gerber, Femtosecond x-ray science, Rep. Prog. Phys. **69**, 443 (2006).

[58] D. Verma, S. M. O. O'Connell, A. J. Feinberg, S. Erukala, R. M. P. Tanyag, C. Bernando, W. Pang, C. A. Saladrigas, B. W. Toulson, M. Borgwardt, N. Shivaram, M. F. Lin, A. AlHaddad, W. Jager, C. Bostedt, P. Walter, O. Gessner, and A. F. Vilesov, Shapes of rotating normal fluid 3He versus superfluid 4He droplets in molecular beams, Phys. Rev. B **102**, 014504 (2020).

[59] R. M. P. Tanyag, C. Bernando, C. F. Jones, C. Bacellar, K. R. Ferguson, D. Anielski, R. Boll, S. Carron, J. P. Cryan, L. Englert *et al.*, Communication: X-ray coherent diffractive imaging by immersion in nanodroplets, Struct. Dyn. **2**, 051102 (2015).

[60] A. J. Feinberg, D. Verma, S. M. O. O'Connell-Lopez, S. Erukala, R. M. P. Tanyag, W. Pang, C. A. Saladrigas, B. W. Toulson, M. Borgwardt, N. Shivaram *et al.*, Aggregation of solutes in bosonic versus fermionic quantum fluids, Sci. Adv. **7**, eabk2247 (2021).

[61] M. Hoener, C. Bostedt, H. Thomas, L. Landt, E. Eremina, H. Wabnitz, T. Laarmann, R. Treusch, A. R. B. d. Castro, and T. Möller, Charge recombination in soft x-ray laser produced nanoplasmas, J. Phys. B **41**, 181001 (2008).

[62] D. Rupp *et al.*, Recombination-Enhanced Surface Expansion of Clusters in Intense Soft X-Ray Laser Pulses, Phys. Rev. Lett. **117**, 153401 (2016).

[63] T. V. Liseykina and D. Bauer, Plasma-Formation Dynamics in Intense Laser-Droplet Interaction, Phys. Rev. Lett. **110**, 145003 (2013).

[64] H. Thomas *et al.*, Explosions of Xenon Clusters in Ultraintense Femtosecond X-Ray Pulses from the LCLS Free Electron Laser, Phys. Rev. Lett. **108**, 133401 (2012).

[65] K. Ishikawa and T. Blenski, Explosion dynamics of rare-gas clusters in an intense laser field, Phys. Rev. A **62**, 063204 (2000).

[66] B. N. Breizman, A. V. Arefiev, and M. V. Fomyts'kyi, Nonlinear physics of laser-irradiated microclusters, Phys. Plasmas **12**, 056706 (2005).

[67] D. D. Hickstein, F. Dollar, J. A. Gaffney, M. E. Foord, G. M. Petrov, B. B. Palm, K. E. Keister, J. L. Ellis, C. Ding, S. B. Libby, J. L. Jimenez, H. C. Kapteyn, M. M. Murnane, and W. Xiong, Observation and Control of Shock Waves in Individual Nanoplasmas, Phys. Rev. Lett. **112**, 115004 (2014).

[68] R. S. Berry, S. A. Rice, and J. Ross, *Physical Chemistry*, 2nd ed. (Oxford University Press, New York, 2000), p. 828.